ACS APPLIED MATERIALS & INTERFACES

Research Article

www.acsami.org

High-Performing Thin-Film Transistors in Large Spherulites of Conjugated Polymer Formed by Epitaxial Growth on Removable Organic Crystalline Templates

Jae Yoon Kim,[†,♦] Da Seul Yang,[†,♦] Jicheol Shin,[†] David Bilby,[‡] Kyeongwoon Chung,[‡] Hyun Ah Um,[†] Jaehee Chun,[§] Seungmoon Pyo,[§] Min Ju Cho,*[,†] Jinsang Kim,*[,‡] and Dong Hoon Choi*[,†]

[†]Department of Chemistry, Research Institute for Natural Sciences, Korea University, 5 Anam-dong, Sungbuk-gu, Seoul 136-701, Republic of Korea

[‡]Department of Materials Science and Engineering, Macromolecular Science and Engineering, University of Michigan, Ann Arbor, Michigan 48109, United States

[§]Department of Chemistry, Konkuk University, 1 Hwayang-dong, Kwangjin-gu, Seoul 143-701, Republic of Korea

Supporting Information

ABSTRACT: Diketopyrrolopyrrole (DPP)-based conjugated polymer **PDTDPPQT** was synthesized and was used to perform epitaxial polymer crystal growth on removable 1,3,5-trichlorobenzene crystallite templates. A thin-film transistor (TFT) was successfully fabricated in well-grown large spherulites of **PDTDPPQT**. The charge carrier mobility along the radial direction of the spherulites was measured to be 5.46−12.04 $cm^2\ V^{-1}\ s^{-1}$, which is significantly higher than that in the direction perpendicular to the radial direction. The dynamic response of charge transport was also investigated by applying a pulsed bias to TFTs loaded with a resistor (~20 MΩ). The charge-transport behaviors along the radial direction and perpendicular to the radial direction were investigated by static and dynamic experiments through a resistor-loaded (RL) inverter. The RL inverter made of **PDTDPPQT**-based TFT operates well, maintaining a fairly high switching voltage ratio ($V_{out}^{ON}/V_{out}^{OFF}$) at a relatively high frequency when the source-drain electrodes are aligned parallel to the radial direction.

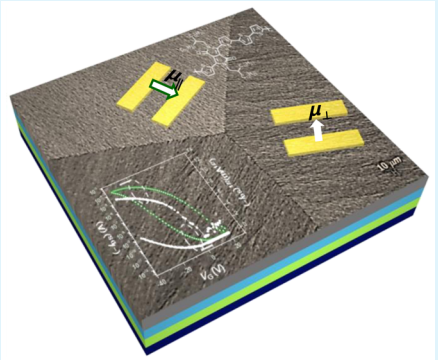

KEYWORDS: *conjugated polymer, diketopyrrolopyrrole, epitaxy, alignment, thin-film transistor*

INTRODUCTION

A number of studies have described that the molecular orientation and molecular packing modes of conjugated polymer chains significantly affect the overall performance of organic field-effect transistors (OFETs). In particular, intramolecular charge transport, rather than hopping transport, is already well-recognized as an important attribute to enhance the charge carrier mobility in semiconducting polymers.[1,2] On the basis of experimental and theoretical research, various crystalline, thin-film forming methods such as solution-shearing,[3] mechanical stretching and rubbing,[4−6] the Langmuir−Blodgett technique,[7,8] dip coating,[9] drop-casting onto inclined substrates,[10] directional epitaxial crystallization,[11−17] and so on[18−20] have been employed for achieving macroscopically aligned polymer films.

However, in spite of the noticeable improvement in carrier mobility in aligned polymer films, the methods required for alignment are relatively time-consuming and require nonstandard equipment or instrumentation compared to the conventional spin-coating method. To overcome those disadvantages, Müller et al. recently devised a one-step epitaxial method to obtain uniaxial alignment of poly(3-hexylthiophene) (P3HT) crystallite.[21] Simply spin-coating a polymer solution with a carrier solvent such as chlorobenzene and a crystallizable solvent such as 1,3,5-trichlorobenzene (TCB) allowed crystallization of the P3HT polymer epitaxially on crystalline needles of TCB. This method allows for the reproducible fabrication of thin films bearing well-ordered P3HT spherulites without any additional investment in equipment, treatment, or time. The TCB crystalline needles, which behave as *microscopic templates* for controlling the directional crystallization of polymer chains, could simply be removed under vacuum (~1×10^{-2} Torr) to isolate the pure semiconducting polymer crystalline film. Therefore, TCB crystalline needles can be called "removable molecular crystallite template." In the past, most of the above-mentioned studies have been carried out using the well-known semiconducting polymer such as PCPDTPBT, PFO, F8BT, and indolocarbazole-containing polymer.[21,22] However, the charge-transport properties of P3HT and other polymers in literature

Received: March 15, 2015
Accepted: June 1, 2015
Published: June 1, 2015

DOI: 10.1021/acsami.5b02265
ACS Appl. Mater. Interfaces 2015, 7, 13431−13439

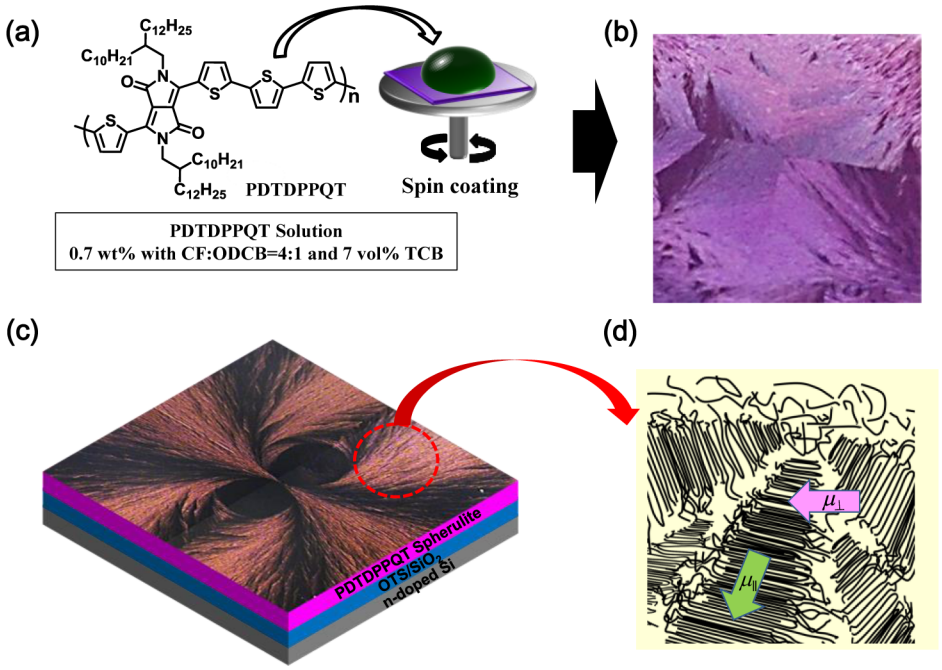

Figure 1. (a) Chemical structure of **PDTDPPQT** and schematic illustration of one-step epitaxial polymer crystal growth via spin coating reported here. (b) The surface of spin-coated film bearing some spherulitic domains. (c) Illustration of a single **PDTDPPQT** spherulite. (d) Detailed schematic diagram of a part of polymer spherulite. $\mu_{\parallel}$ and $\mu_{\perp}$ are the carrier mobilities parallel and perpendicular to the radial direction, respectively.

are notably inferior to those of the conjugated polymers reported in most recent literature.[23]

Among various high-performing semiconducting conjugated polymers, diketopyrrolopyrrole (DPP)-based polymers are considered as materials with great potential for future flexible electronic (e.g., thin-film transistor (TFTs))[23,24] and optoelectronic (e.g., photovoltaics) devices,[24] largely because of their highly crystalline nature and remarkably high charge-transport properties.

In this work, we first employed a DPP-based conjugated polymer, namely, **PDTDPPQT** (Figure 1), to conduct epitaxial polymer crystal growth (EPCG) on removable TCB crystallite templates. By considering the solubility of the **PDTDPPQT**, well-defined polymer spherulites, large enough for fabricating TFTs, were successfully prepared by optimizing the composition of carrier solvent and TCB in the solvent mixture. When applying this EPCG technique to fabricate active channels in TFTs and investigating their unique charge-transport property, the maximum carrier mobility ($\mu_{\parallel}^{max}$ = 12.04 cm^2 V^{-1} s^{-1}) along the radial direction was measured to be almost 3−4 times higher than that in the perpendicular direction ($\mu_{\perp}^{max}$ = 3.66 cm^2 V^{-1} s^{-1}).

On the basis of the results of the charge-transport properties in the spherulite, we fabricated a simple resistor-loaded (RL) inverter and performed experiments for monitoring charge-transport dynamics, which is important in practical thin-film transistors. It was determined that a higher mobility device (TFT-∥) whose source-drain electrode is aligned to the radial direction could display higher ON/OFF voltage switching ratio at a high-frequency bias voltage. The TFT-∥-based RL-inverter device exhibited a short rising time (~0.59 ms) and a falling time of 1.29 ms. The rising time is much smaller than the times observed in RL inverters made from TFT-⊥, whose source-drain electrode is aligned perpendicularly to the radial direction.

EXPERIMENTAL SECTION

Instrumentation. ^{1}H NMR spectra were recorded on a Varian Mercury NMR 300 MHz spectrometer and referenced to deuterated chloroform purchased from Cambridge Isotope Laboratories. The molecular weight of the polymer was determined by gel permeation chromatography (GPC, Waters 515 HPLC pump, Waters 410 RI differential refractometer detector, 2x PLgel Mixed-B, Waters, Milford, MA) using polystyrene as the standard, chloroform as an eluent (T = 35 °C), and 1,2,4-trichlobenzene at 150 °C. Optical micrographic images were obtained using a KSM-BA3(T) microscope (Samwon). Grazing incidence wide-angle X-ray diffraction (GIXD) measurements were performed at the 9A (U-SAXS) beamline (energy = 11.105 keV, pixel size = 79.6 mm, λ = 1.12 Å, 2θ = 0°~20°) at the Pohang Accelerator Laboratory (PAL). The film samples were fabricated by spin-casting on *n*-octadecyltrichlorosilane (OTS)−SiO_2/Si substrate, followed by drying at 50 °C under vacuum (solvent: chloroform and 1,2-dichlorobenzene (4:1 v/v) in the presence of 1,3,5-trichlorobenzene (TCB), concentration: 7 mg mL^{-1}). Atomic force microscopy (AFM, Advanced Scanning Probe Microscope, XE-100, psia) operating in tapping mode with a silicon cantilever was used to characterize the surface morphologies of the film samples. Scanning electron microscopy (SEM) images were obtained using a Jeol JSM-7001F instrument. The SEM images were acquired at 15.0 kV using platinum-sputtered samples.

Thin-Film Transistor Fabrication and Characterization. Bottom-gate top-contact TFTs were fabricated on a highly n-doped silicon substrate with a 300 nm thick thermally grown SiO_2. The substrates were cleaned sequentially with deionized water, acetone, and isopropanol for 10 min each and then exposed to UV/ozone for 20 min. The SiO_2 dielectric surface was modified with an OTS self-assembled monolayer to enhance its electrical performance. Aligned **PDTDPPQT** films were prepared on the OTS−SiO_2/Si substrate by spin-coating from 0.7 wt % solutions of chloroform and 1,2-dichlorobenzene (4:1 v/v) in the presence of 7 vol % 1,3,5-trichlorobenzene (TCB) at 2000 rpm for 30 s. Source and drain electrodes were thermally evaporated through a shadow mask with a channel width of 200 μm and length of 80 μm. The hole mobilities were extracted in the saturation regime using the relationship $\mu_{sat} = (2I_{DS}L)/(WC(V_G - V_{th})^2)$, where I_{DS} is the saturation drain current, C

DOI: 10.1021/acsami.5b02265
ACS Appl. Mater. Interfaces 2015, 7, 13431−13439

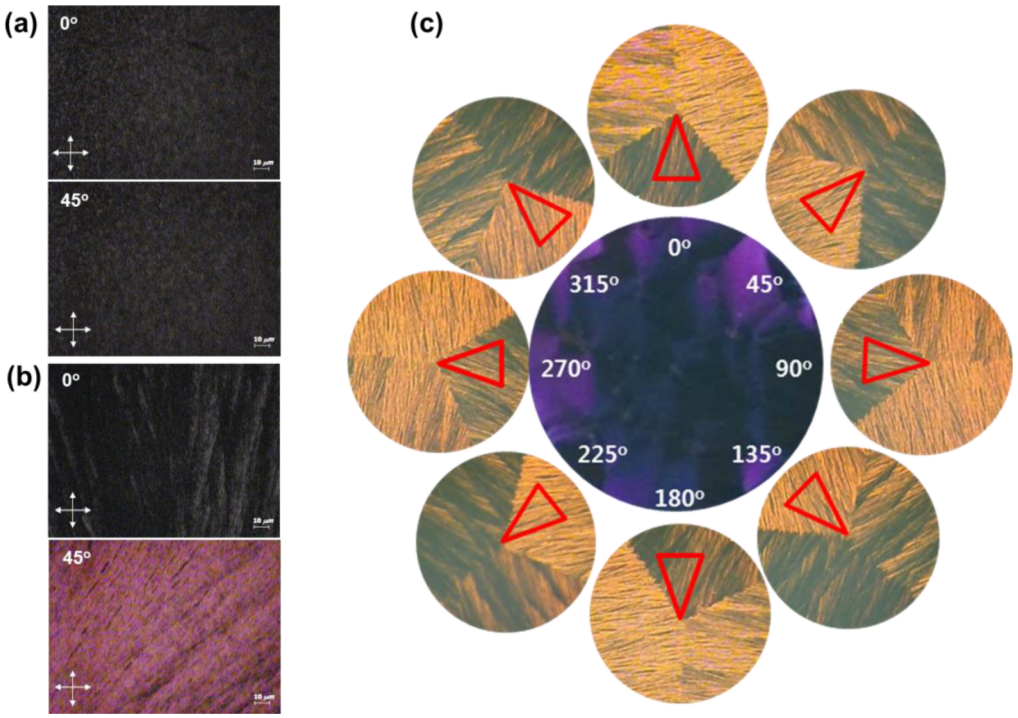

Figure 2. (a–c) Polarized optical micrographs of **PDTDPPQT** films spin-coated from **PDTDPPQT** solutions (a) without and (b, c) with TCB.

is the capacitance (~11.5 nF cm^{-2}) of the silicon oxide dielectric, V_G is the gate bias, and V_{th} is the threshold voltage. All the devices were characterized in air using the Keithley 4200-SCS semiconductor parameter analyzer.

Resistance-Loaded Inverter and Electrical Characterization. For the characterization of static and dynamic responses of the device, we fabricated an RL inverter, a simplified primary logic gate, by connecting the TFTs made from the **PDTDPPQT** with a 20 MΩ load resistor. For the response time measurement, a function generator (RIGOR DG4062) was employed to supply the input square wave gate voltage, and an oscilloscope (RIGOR DS2102) was connected to the output electrode to measure the output voltage signal (V_{OUT}) in ambient conditions when a square wave input signal (V_{IN} = 0 to −60 V) was applied to the device at V_{DD} = −60 V.

RESULTS AND DISCUSSION

Diketopyrrolopyrrole-Based Polymer and Its Molecular Weight. To investigate the EPCG of the DPP-based copolymer, **PDTDPPQT** was synthesized according to our previous reports.[25,26] The number-average molecular weight (M_n) and polydispersity index (PDI) of **PDTDPPQT** were 290 kDa and 11, respectively, which was determined by gel permeation chromatography (GPC) with chloroform as the eluent based on polystyrene standard. High -temperature GPC was also performed in 1,2,4-trichlorobenzene as the eluent at 150 °C (M_n = 29 kDa, PDI = 2.4) (Supporting Information, Figure S1).

Epitaxial Polymer Crystal Growth. Selection of the correct solvent and composition of TCB for dissolving **PDTDPPQT** is very crucial to promote crystallization and control the size of the spherulites during spin-coating. We prepared the polymer solution by dissolution into a mixture of chloroform and 1,2-dichlorobenzene (4:1 v/v) in the presence of TCB. Chloroform was selected as a good solvent having a low boiling point, whereas 1,2-dichlorobenzene was used as the high boiling point solvent. The high boiling point solvent is expected to undergo slow evaporation providing enough time for the polymer to increase in crystallinity and form highly crystalline domains.[2,27,28]

At a fixed composition of mixed solvents (e.g., chloroform/1,2-dichlorobenzene = 4:1 v/v) and solution concentration (0.7 wt %) of the polymer, we varied the concentration of TCB to investigate its effect on crystallization and the size of spherulites. Eventually, the best concentration of TCB was optimized for successful epitaxial crystal growth of the polymer. As shown in Supporting Information, Figure S2, we fabricated five different films by spin coating with polymer solutions containing (i) 0, (ii) 1, (iii) 4, (iv) 7, and (v) 10 vol % TCB. A spherulitic crystallite domain diameter of at least 100 μm was desired, as this would be sufficient to cover the active channel area in a TFT. While the films fabricated using the polymer solutions with 4, 7, and 10 vol % TCB showed fairly large spherulitic Maltese-cross patterns visible to the naked eye, the solution with 1 vol % TCB did not show any uniform crystalline patterns. This can be explained by the fact that a relatively small amount of TCB (e.g., 1 vol %) does not serve as an epitaxial crystallization template but only acts as a high boiling point solvent additive for retarding the drying process.[21]

Atomic force microscopy (AFM) measurements were conducted in tapping mode (Supporting Information, Figure S3) to investigate the surface topographies of the crystalline polymer films prepared with solutions (iii)–(v). For solution (iii), the presence of too many nucleation sites blocks the formation of large areas of spherulitic domains. For solution (v) (Figure S3c), however, a few large, dark areas were observed on the surface of the polymer film. It can be postulated that the dark areas on the film surface might be located in lower areas or occupied with disordered amorphous regions, which can increase the energy barrier between lamellar crystallites or increase the density of potential charge traps. Accordingly, they can hamper charge carrier transport in the active channel area of TFTs.[29] This hypothesis will be discussed in more detail with the carrier mobilities displayed in Figure 6. Ultimately, we

DOI: 10.1021/acsami.5b02265
ACS Appl. Mater. Interfaces 2015, 7, 13431–13439

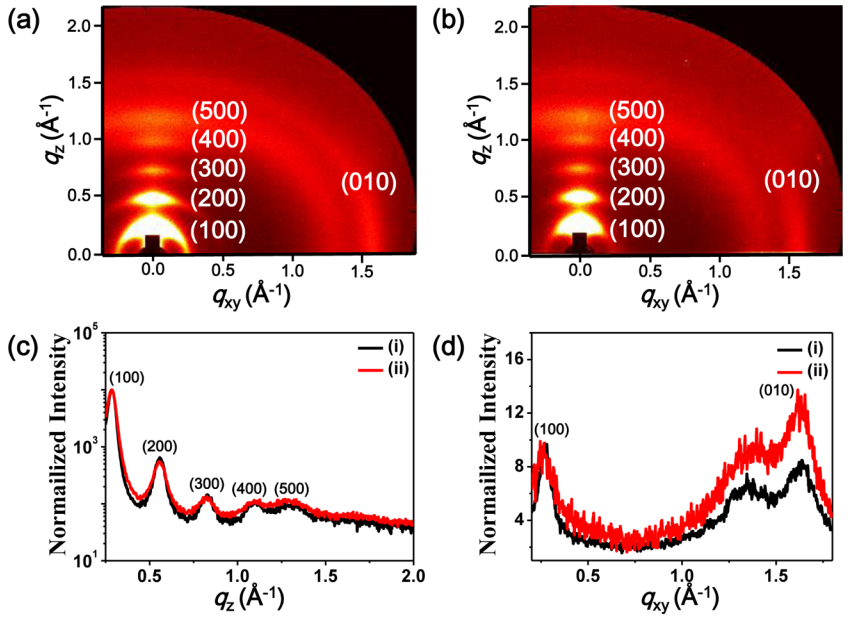

Figure 3. 2D-GIXD patterns for a plane of incidence (a) parallel and (b) perpendicular to the radial direction of spherulite. (c) Out-of-plane and (d) in-plane profiles for a plane of incidence (i) parallel and (ii) perpendicular to the radial direction.

selected the solution with 7 vol % TCB as the best for achieving densely packed crystalline thin films on the substrates. Using 7 vol % TCB, the spin-coated films displayed uniform surface morphology as well as highly oriented lamellar crystalline domains over hundreds of square micrometers, as shown in Supporting Information, Figure S4.

Polarized optical microscopy images of the spin-coated films were obtained and are displayed in Figure 2a–c. Although the spin-coated film made with solution (i) (i.e., 0 vol % TCB) was rotated with respect to the axis of the crossed polar, only dark images were obtained, which indicates a random orientation of the polymer chains or elongated lamellar crystallites (Figure 2a).

However, in the film fabricated with solution (iv) (7 vol % TCB), bright images were obtained owing to the optical birefringence observed periodically when rotating the axis of the aligned direction of the long axis of lamellar crystallites by 45° to the crossed-polar axis, indicating the existence of ordered, nanocrystalline lamellae in the localized area. This phenomenon is attributed to epitaxial crystal growth of the polymer on top of the TCB template during solvent evaporation.

GIXD and Atomic Force Microscopy Analysis. We employed GIXD to confirm the polymer chain and crystallite packing of the aligned **PDTDPPQT** film and compare it to conventional isotropic spin-coated films prepared without the crystallizable solvent additive TCB. The reference isotropic film sample prepared by spin-coating a **PDTDPPQT** solution without TCB exhibited dual internal morphology on the substrate with (100) and (010) Bragg peaks observed in both the out-of-plane and in-plane profiles (Supporting Information, Figure S5), indicating the presence of a mixture of face-on and edge-on oriented crystallites in the solid film. The film showed three orders of interlamellar stacking peaks (e.g., (100), (200), and (300)) in the out-of-plane profile. For instance, a $d_{(100)}$-spacing of 22.46 Å was observed at 2θ = 2.85° as well as the (100) diffraction peak (2θ = 2.82°; $d_{(100)}$ = 22.68 Å) along the q_{xy} axis direction in the in-plane profile. The (010) diffraction peak at 2θ = 17.05° can be assigned to a $\pi-\pi$ stacking distance of 3.79 Å.

In Figure 3, the two-dimensional (2D) GIXD data are shown for a better understanding of the morphology of the aligned polymer films. Anisotropic alignment in the films is clearly observed when the localized alignment direction of the lamellae crystallites is perpendicular or parallel to the plane of X-ray beam incidence. When the crystallite alignment direction was almost parallel to the plane of incidence, a relatively strong third-order diffraction peak was observed because of inter-lamellar stacking along the q_z axis. The (010) diffraction peak ($d^{\parallel}_{(010)}$ = 3.80 Å) was observed more clearly for the film produced with TCB than for the conventional spin-coated film (e.g., $d_{(010)}$ = 3.80 Å; Figure 3d).

The (100) diffraction peak was also observed in the in-plane profile, but the intensity of this diffraction peak was much smaller than in the out-of plane mode (Figure 3d(i)). Although a small extent of face-on chain arrangements can be expected, these results could be considered as evidence of well-defined $\pi-\pi$ stacking interactions between adjacent polymer chains, resulting in predominantly edge-on chain orientation on the substrate.

However, when the long axis of the lamellar crystallite was perpendicular to the plane of incidence, very weak and less-defined (100) diffraction peaks were observed in the in-plane profiles. When the plane of incidence is perpendicular to the radial direction, a higher intensity of (010) diffraction was obviously observed in a q_{xy} axis, which is consistent with the results in the literature (Figure 3d(ii)).[9] This indicates that the π-stacking direction of lamella crystallites is parallel to the radial direction as was illustrated in Figure 1d. Combining the results from the two in-plane profiles, it is suggested that the epitaxially grown lamellar crystallites were aligned along a radial direction, which is strong evidence for macroscopic alignment in a small localized area.

As shown in Figure 4a,b, tapping mode atomic force microscopy (AFM) was employed to investigate the surface topography of aligned polymer films made with the

DOI: 10.1021/acsami.5b02265
ACS Appl. Mater. Interfaces 2015, 7, 13431–13439

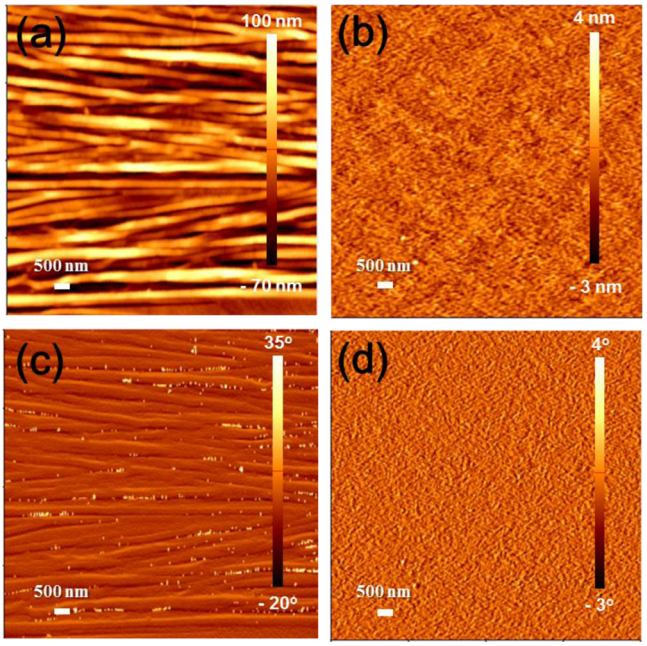

Figure 4. AFM height (upper) and phase (lower) images of **PDTDPPQT** films fabricated by EPCG using 7 vol % TCB (a, c) and spin-coating without adding TCB (b, d).

PDTDPPQT solution with 7 vol % TCB and spin-coated films without using TCB. The nodular morphology of the isotropic **PDTDPPQT** film is shown in Figure 4b and is similar to the surface images of high molecular weight conjugated polymer films reported in the literature (average roughness <3 nm).[30,31] Compared to the surface image of isotropic films, a distinct change in the height and phase images is observed for the aligned films, with oriented lamellar crystallite structures being apparent with an average width of ~200 nm. It was evident that a disordered amorphous region exists between the lamellar crystallites.

Since the crystalline conjugated polymer has relatively complicated structures and various conformations, the microstructure dependence of charge-transport is scarcely studied. This results from the infeasibility of fabricating sufficiently large macroscopic samples with fairly high long-range crystalline order. In this study, we grew sufficiently large well-defined spherulites of **PDTDPPQT**, which allows fabricating TFTs in the corresponding crystalline domain.

Characterization of Thin-Film Transistor. Bottom-gate top-contact (BGTC) TFT devices were fabricated using spherulitic crystalline films of **PDTDPPQT** on OTS−SiO_2/Si substrates with a 300 nm oxide layer. To investigate the unique charge transport in the aligned films, we fabricated two kinds of devices, with the source-drain electrodes parallel (i.e., TFT-||) or perpendicular (i.e., TFT-⊥) to the long axis of lamellar crystallites (Figure 5c, inset). The representative transfer and output characteristics of the TFTs fabricated in spherulites measured at room temperature are illustrated in Figure 5a,b. When the polymer crystallites were grown parallel to the current flow between the source and the drain electrode (i.e., TFT-||), we obtained a high hole mobility of $\mu_{\parallel}^{avg}$ = 7.12 cm^2 V^{-1} s^{-1} ($\mu_{\parallel}^{max}$ = 12.04 cm^2 V^{-1} s^{-1}), whereas a significantly lower value of $\mu_{\perp}^{avg}$ = 2.89 cm^2 V^{-1} s^{-1} ($\mu_{\perp}^{max}$ = 3.66 cm^2 V^{-1} s^{-1}) was measured in TFT-⊥. Although the channel width and length of the device were varied, the same tendency could be observed. (Figure S11 in the Supporting Information). After these values were compared with the mobility (μ_{iso}) of an annealing-free isotropic film device (i.e., TFT-S) prepared by spin coating without TCB, the mobility (μ_{iso}) was found to be close to $\mu_{\perp}$ (μ_{iso} = 2.58 cm^2 V^{-1} s^{-1}, $\mu_{\perp}$ = 2.89 cm^2 V^{-1} s^{-1}). Of greater interest, the annealing-free spherulitic film-based transistor showed ~1.6−2.0 times higher mobility than the thermally annealed thin-film transistor (μ_{iso}^{max} = 3.69 cm^2 V^{-1} s^{-1}, $T_{annealing}$ = 200 °C for 10 min) (Supporting Information, Table S1).

It has already been suggested that the semicrystalline solid-state morphology displayed ordered, nanocrystalline π-stacked lamellae coexisting with disordered amorphous regions that

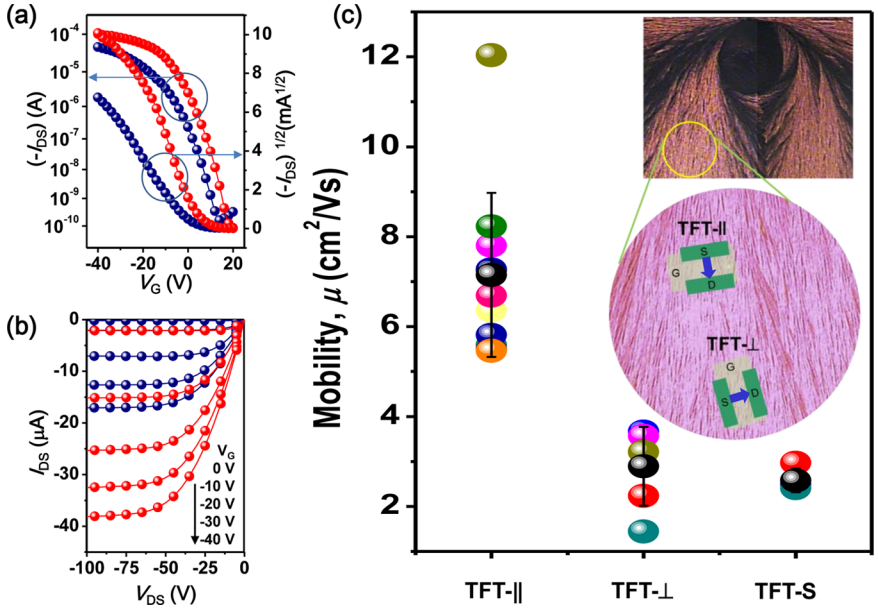

Figure 5. (a) Transfer and (b) output curve (V_{DS} = −100 V) characteristics of the two different TFTs. TFT-|| (red) and TFT-⊥ (blue) *channel width, 200 μm; channel length, 80 μm. (c) Distribution of hole mobilities measured in various devices.

DOI: 10.1021/acsami.5b02265
ACS Appl. Mater. Interfaces 2015, 7, 13431−13439

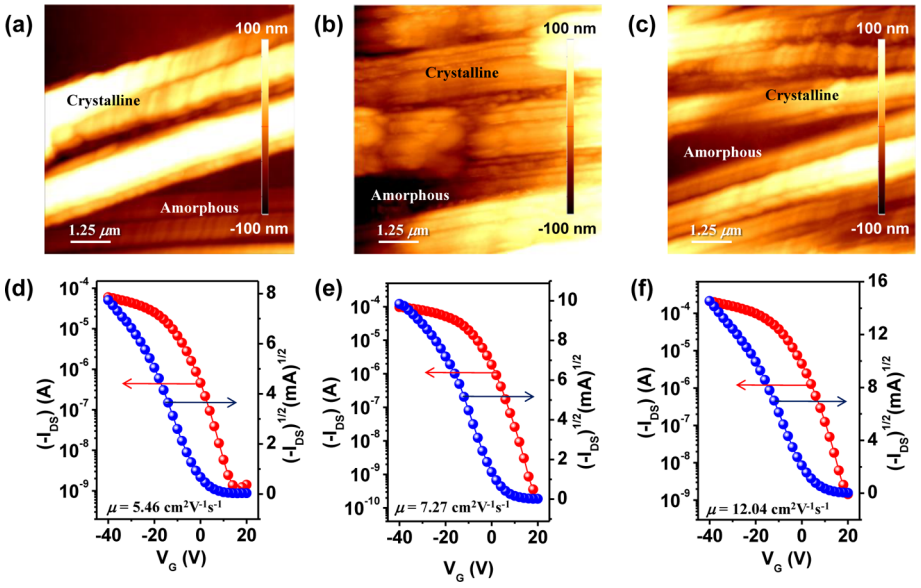

Figure 6. (a–c) Atomic force microscope images of the surfaces of the three TFT-‖ devices. (d–f) Transfer curve (V_{DS} = −100 V) characteristics of the three TFT-‖ devices. *channel width = 200 μm; channel length = 80 μm.

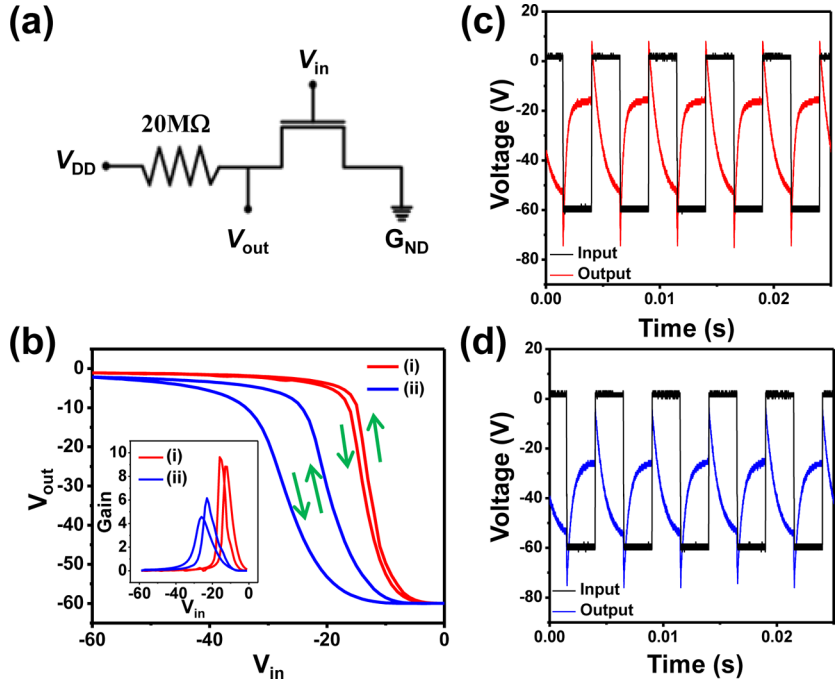

Figure 7. RL inverters made of **PDTDPPQT** polymer. (a) Circuit diagram of RL inverter. (b) Voltage transfer characteristics of the **PDTDPPQT** RL-inverter measured with increasing and decreasing input voltage V_{IN} (V_{DD} = −60 V). (inset) Voltage gain in the inverter as a function of V_{IN}. (i) TFT-‖, (ii) TFT-⊥. (c) Dynamic output voltage response of **PDTDPPQT** RL-inverter made with TFT-‖ when the square wave input voltage was switched at 200 Hz. *W = 200 μm, L = 80 μm. (d) Dynamic output voltage response of **PDTDPPQT** RL-inverter made with TFT-⊥. Output responses were monitored when the input voltage was switched at 200 Hz.

hamper the pure intramolecular charge transport through the repeating units in a conjugated polymer chain over macroscopic distances. Charge carriers in conjugated polymers are inclined to migrate either along the growing direction of lamellar crystallites, by hopping through π-stacked polymer chains, or perpendicular to the long axis of lamellar crystallites along conjugated polymer chains before crossing the amorphous region.[22] Charge transport through the amorphous inter-lamellar zone is most likely a combination of hopping between disordered segments on neighboring chains and intrachain transport where a single chain (i.e., tie chain) extends across adjacent lamellae. Although the semicrystalline region in which charge carriers travel consisted of ordered crystalline and disordered amorphous region together in the film state, the charge transport in TFT-‖ was observed to be much faster than that of TFT-⊥. Therefore, a much lower $\mu_{\perp}$ might be because of the presence of disordered regions between the lamellar crystallites, which implies a large barrier energy for long-range charge transport.

DOI: 10.1021/acsami.5b02265
ACS Appl. Mater. Interfaces 2015, 7, 13431−13439

We were so curious about the large variation in the mobility in TFT-|| devices from 5.46 to 12.04 $cm^2 V^{-1} s^{-1}$, as shown in Figure 5c and Supporting Information, Table S2. To answer this question, we selected three TFT-|| devices to observe the surfaces of the active channels using AFM. In Figure 6a–c, it was unambiguously observed that the density of lamellar crystallites in the channels showed significant difference; the device exhibiting 12.04 $cm^2 V^{-1} s^{-1}$ contains a high density of crystallites compared to the device displaying lower carrier mobility. Therefore, even though the charge-hopping mechanism in TFT-|| boosted the carrier mobility up to two-digit numbers, the density of the crystallites through the channel is very critical to the high-performing charge-transport behavior in the corresponding devices. The measured mobilities in the three devices could partly support the hypothesis about the existence of disordered region in the dark area.[29]

Characterization of the Resistor-Loaded Inverter. To investigate the static and dynamic response of the TFTs, simple RL inverters were fabricated by connecting a load resistor (20 MΩ) as shown in Figure 7a. The voltage transfer characteristics ($V_{IN} - V_{OUT}$) and corresponding gain of the RL inverters based on the two different TFTs (e.g., TFT-|| and TFT-⊥) for forward (i.e., from 0 to −60 V) and reverse (i.e., from −60 to 0 V) scans at V_{DD} = −60 V are shown in Figure 7b. Clearly, the output voltage switched from the "1" state (−60 V) to the "0" state (ca. −1.06 to −2.15 V) when the input signal was swept from −60 to 0 V.

Compared to the TFT-||-based RL inverter, the TFT-⊥-based inverter displayed larger hysteresis behavior (ΔV = 7.0 V) than that (ΔV = 1.0 V) of TFT-||-based RL inverter. It may be caused by lower mobility of TFT-⊥ compared to that of TFT-|| device.[32] Besides the low hysteresis behavior of TFT-||-based RL inverter, it displayed a much larger voltage gain (i.e., dV_{OUT}/dV_{IN}) of almost 9.6 at V_{IN} = −16 V, which showed a clear switching response.

The dynamic response behaviors of the RL inverters made of the two types of TFTs at a frequency of 200 Hz are shown in Figure 7c,d. Although the device structures were not fully optimized for a switching response, the devices demonstrated a modest switching behavior with different response times. As can be seen in Figure 7c,d, when the square wave input bias (V_{IN}) (between 0 and −60 V) is applied at 200 Hz, the output voltage (V_{OUT}) was switched from the ON to OFF state and vice versa in the inverters.

To investigate the relationship between carrier mobility in TFT and the dynamic response, we measured the switching response time of RL inverters with a 200 Hz input voltage signal where the two devices operate well. Rising time (τ_r) and falling time (τ_f) are defined as the times required for increasing from 10% to 90% of the output level or falling from 90% to 10%, respectively. The falling times of the two inverters were almost identical and were 1.19–1.29 ms [i.e., τ_f (TFT-||) = 1.29 ms ; τ_f (TFT-⊥) = 1.19 ms]. On the contrary, the rising times of the two devices at 200 Hz were significantly different; the rising time of the TFT-||-based inverter (τ_r = 0.59 ms) is much smaller than that of the TFT-⊥-based inverter (τ_r = 1.01 ms). The rising time was found to be inversely proportional to the carrier mobility measured in the static states. TFT-||-based inverter did display a shorter rising time than the TFT-⊥-based inverter owing to much higher carrier mobility. The dynamic responses of the inverter made of TFT-⊥ and TFT-|| were examined at various frequencies of V_{IN}, as shown in Figures S12 and S13 (Supporting Information). The inverter based on TFT-|| whose mobility is more than two times higher than TFT-⊥ shows a clearer switching response up to 1 kHz.

In Figure 8, output voltages at the ON and OFF states of **PDTDPPQT**-based RL-inverter were investigated as a function

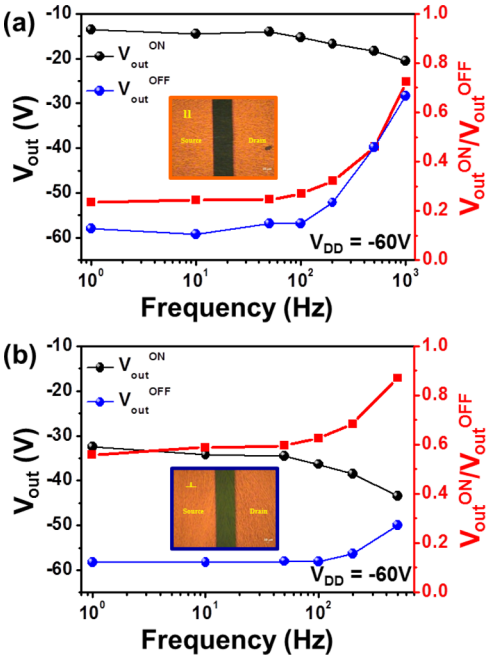

Figure 8. Output voltages at ON and OFF states of **PDTDPPQT**-based RL-inverter as a function of switching frequency. *Square: $V_{out}^{ON}/V_{out}^{OFF}$ (a) RL-inverter made with TFT-||. (b) RL-inverter made with TFT-⊥.

of input voltage pulse frequency. The inverter made of TFT-|| operates well up to 1000 Hz, maintaining a fairly high switching voltage ratio ($V_{out}^{ON}/V_{out}^{OFF}$) even at a high frequency of 200–1000 Hz. However, owing to the much lower mobility of TFT-⊥, the inverter exhibited much smaller $V_{out}^{ON}/V_{out}^{OFF}$ ratio in the measured frequency range. In brief, as a result of the dynamic experiment using RL-inverter it was determined that TFT-|| with much higher carrier mobility displayed markedly better switching response and higher voltage gain with small hysteresis behavior.

CONCLUSIONS

EPCG using DPP-based conjugated polymer **PDTDPPQT** was conducted on removable TCB crystallite templates. Large polymer spherulites could be prepared, and TFTs were successfully fabricated in spherulites. The charge carrier mobility along the radial direction of the spherulite was measured to be 5.46–12.04 $cm^2 V^{-1} s^{-1}$, which is significantly higher than that of spherulites perpendicular to the radial direction. The variation in the mobility was found to be due to density of lamellar crystallites in the channels. Although a carrier mobility of over 1 × 10 $cm^2 V^{-1} s^{-1}$ was observed in TFT-||, the charge-transport behavior was found to be dependent on the density of the crystallites through the channel in the devices.

The dynamic response of charge transport was also investigated by applying a pulsed bias to TFTs loaded with a resistor (~20 MΩ). The RL inverter made of **PDTDPPQT**-based TFT operates well, maintaining a fairly high switching voltage ratio ($V_{out}^{ON}/V_{out}^{OFF}$) at a relatively high frequency

DOI: 10.1021/acsami.5b02265
ACS Appl. Mater. Interfaces 2015, 7, 13431–13439

when the source-drain electrodes are aligned parallel to the radial direction. It was determined that TFT-|| showing much higher carrier mobility displayed markedly better switching response and higher voltage gain.

■ ASSOCIATED CONTENT

Supporting Information

Synthesis and characterization of **PDTDPPQT**, GPC chromatogram, optical miscroscopic images, AFM images, SEM image, device performance data, TFT data of unannealed and annealed film without using TCB, dynamic output voltage response of RL-inverter. The Supporting Information is available free of charge on the ACS Publications website at DOI: 10.1021/acsami.5b02265.

■ AUTHOR INFORMATION

Corresponding Authors

*E-mail: chominju@korea.ac.kr. (M.J.C.)
*E-mail: jinsang@umich.edu. (J.K.)
*E-mail: dhchoi8803@korea.ac.kr. (D.H.C.)

Author Contributions

♦These authors contributed equally.

Notes

The authors declare no competing financial interest.

■ ACKNOWLEDGMENTS

This research was supported by National Research Foundation of Korea (NRF2012R1A2A1A01008797) and by Key Research Institute Program (NRF201200020209). We are grateful to Pohang Accelerator Laboratory (Pohang, Korea) for allowing us to conduct the grazing incidence X-ray diffraction (GIXD) measurements. J.K. acknowledges the financial support from MCubed and U.S. Department of Energy (DOE), Office of Basic Energy Sciences, as part of the Center for Solar and Thermal Energy Conversion in Complex Materials, an Energy Frontier Research Center (DE-SC0000957).

■ REFERENCES

(1) Wang, S.; Kappl, M.; Liebewirth, I.; Müller, M.; Kirchhoff, K.; Pisula, W.; Müllen, K. Organic Field-Effect Transistors based on Highly Ordered Single Polymer Fibers. *Adv. Mater.* **2012**, *24*, 417−420.

(2) Yao, Y.; Dong, H.; Hu, W. Ordering of Conjugated Polymer Molecules: Recent Advances and Perspectives. *Polym. Chem.* **2013**, *4*, 5197−5205.

(3) Giri, G.; Verploegen, E.; Mannsfeld, S. C. B.; Atahan-Everenk, S.; Kim, D. H.; Lee, S. Y.; Becerril, H. A.; Aspuru-Guzik, A.; Toney, M. F.; Bao, Z. Tuning Charge Transport in Solution-Sheared Organic Semiconductors using Lattice Strain. *Nature* **2011**, *480*, 504−509.

(4) Tremel, K.; Fischer, F. S. U.; Kayunkid, N.; Pietro, R. D.; Tkachov, R.; Kiriy, A.; Neher, D.; Ludwigs, S.; Brinkmann, M. Charge Transport Anisotropy in Highly Oriented Thin Films of the Acceptor Polymer P(NDI2OD-T2). *Adv. Energy. Mater.* **2014**, *4*, 1301659.

(5) O'Connnor, B. T.; Reid, O. G.; Zhang, X.; Kline, R. J.; Ritcher, L. J.; Gundlach, D. J.; DeLongChamp, D. M.; Toney, M. F.; Kopidakis, N.; Rumbles, G. Morphological Origin of Charge Transport Anisotropy in Aligned Polythiophene Thin Films. *Adv. Funct. Mater.* **2014**, *24*, 3422−3431.

(6) Laure, B.; Nicolas, L.; Thomas, H.; Rony, B.; Martin, B. Large Scale Alignment and Charge Transport Anisotropy of pBTTT Films Oriented by High Temperature Rubbing. *Macromolecules* **2013**, *46*, 4014−4023.

(7) Xu, G.; Bao, Z.; Groves, J. T. Langmuir-Blodgett Films of Regioregular Poly(3-hexylthiophene) as Field-Effect Transistors. *Langmuir* **2000**, *16*, 1834−1841.

(8) Paloheimo, J.; Kuivalainen, P.; Stubb, H.; Vuorimaa, E.; Yli-Lahti, P. Molecular Field-Effect Transistors Using Conducting Polymer Langmuir-Blodgett Films. *Appl. Phys. Lett.* **1990**, *56*, 1157−1159.

(9) Tsao, H. N.; Cho, D.; Andreasen, J. W.; Rouhanipour, A.; Breiby, D. W.; Pisula, W.; Müllen, K. The Influence of Morphology on High-Performance Polymer Field-Effect Transistors. *Adv. Mater.* **2009**, *21*, 209−212.

(10) Rivnay, J.; Jimison, L. H.; Northurp, J. E.; Toney, M. F.; Noriega, R.; Lu, S.; Marks, T. J.; Facchetti, A.; Salleo, A. Large Modulation of Carrier Transport by Grain-boundary Molecular Packing and Microstructure in Organic Thin Gilms. *Nat. Mater.* **2009**, *8*, 952−958.

(11) Hartmann, L.; Tremel, K.; Uttiya, S.; Crossland, E.; Ludwigs, S.; Kayunkid, N.; Bergnat, C.; Brinkmann, M. 2D Versus 3D Crystalline Order in Thin Films of Regioregular Poly(3-hexylthiophene) Oriented by Mechanical Rubbing and Epitaxy. *Adv. Funct. Mater.* **2011**, *21*, 4047−4057.

(12) Jimison, L. H.; Toney, M. F.; McCulloch, I.; Heeney, M.; Salleo, A. Charge-Transport Anisotropy Due to Grain Boundaries in Directionally Crystallized Thin Films of Regioregular Poly(3-hexylthiophene). *Adv. Mater.* **2009**, *21*, 1568−1572.

(13) Zen, A.; Saphiannikova, M.; Neher, D.; Grenzer, J.; Grigorian, S.; Pietch, U.; Asawapirom, U.; Janietz, S.; Scherf, U.; Lieberwirth, I.; Wegner, G. Effect of Molecular Weight on the Structure and Crystallinity of Poly(3-hexylthiophene). *Macromolecules* **2006**, *39*, 2162−2171.

(14) Brinkmann, M.; Gonthier, E.; Bogen, S.; Tremel, K.; Ludwigs, S.; Hugnagel, M.; Sommer, M. Segregated versus Mixed Interchain Stacking in Highly Oriented Films of Naphthalene Diimide Bithiophene Copolymers. *ACS Nano* **2012**, *11*, 10319−10326.

(15) Brinkmann, M.; Rannou, P. Effect of Molecular Weight on the Structure and Morphology of Oriented Thin Films of Regioregular Poly(3-hexylthiophene) Grown by Directional Epitaxial Solidification. *Adv. Funct. Mater.* **2007**, *17*, 101−108.

(16) Brinkmann, M.; Wittmann, J.-C. Orientation of Regioregular Poly(3-hexylthiophene) by Directional Solidification: A Simple Method to Reveal the Semicrystalline Structure of a Conjugated Polymer. *Adv. Mater.* **2006**, *18*, 860−863.

(17) Brinkmann, M. Directional Epitaxial Crystallization and Tentative Crystal Structure of Poly(9,9¢-di-n-octyl-2,7-fluorene). *Macromolecules* **2007**, *40*, 7532−7541.

(18) Tseng, H.-R.; Phan, H.; Luo, C.; Wang, M.; Perez, L. A.; Patel, S. N.; Ying, L.; Kramer, E. J.; Nguyen, T.-Q.; Bazan, G. C.; Heeger, A. J. High-Mobility Field-Effect Transistors Fabricated with Macroscopic Aligned Semiconducting Polymers. *Adv. Mater.* **2014**, *26*, 2993−2998.

(19) Lee, M. J.; Gupta, D.; Zhao, N.; Heeney, M.; McCulloch, I.; Sirringhaus, H. Anisotropy of Charge Transport in a Uniaxially Aligned and Chain-Extended, High-Mobility, Conjugated Polymer Semiconductor. *Adv. Funct. Mater.* **2011**, *21*, 932−940.

(20) Tseng, H.-R.; Ying, L.; Hsu, B. B. Y.; Perez, L. A.; Takacs, C. J.; Bazan, G. C.; Heeger, A. J. High Mobility Field Effect Transistors Based on Macroscopically Oriented Regioregular Copolymers. *Nano Lett.* **2012**, *12*, 6353−6357.

(21) Müller, C.; Aghamohammadi, M.; Himmelberger, S.; Sonar, P.; Garriga, M.; Salleo, A.; Compoy-Quiles, M. One-Step Macroscopic Alignment of Conjugated Polymer Systems by Epitaxial Crystallization during Spin-Coating. *Adv. Funct. Mater.* **2013**, *23*, 2368−2377.

(22) Park, K. S.; Salunkhe, S. M.; Lim, I.; Cho, C.-G.; Han, S.-H.; Sung, M. M. High-Performance Air-Stable Single-Crystal Organic Nanowires Based on a New Indolocarbazole Derivative for Field-Effect Transistors. *Adv. Mater.* **2013**, *25*, 3351−3356.

(23) Holiday, S.; Donaghey, J. E.; McCulloch, I. Advances in Charge Carrier Mobilities of Semiconducting Polymers Used in Organic Transistors. *Chem. Mater.* **2014**, *26*, 647−663.

(24) Li, Y.; Sonar, P.; Murphy, L.; Hong, W. High Mobility Diketopyrrolopyrrole (DPP)-based Organic Semiconductor Materials

DOI: 10.1021/acsami.5b02265
ACS Appl. Mater. Interfaces 2015, 7, 13431−13439

for Organic Thin Film Transistors and Photovoltaics. *Energy Environ. Sci.* **2013**, *6*, 1684−1710.
(25) Li, W.; Hendriks, K. H.; Furlan, A.; Roelofs, W. S. C.; Wienk, M. M.; Janssen, R. A. J. Universal Correlation between Fibril Width and Quantum Efficiency in Diketopyrrolopyrrole-Based Polymer Solar Cells. *J. Am. Chem. Soc.* **2013**, *135*, 18942−18948.
(26) Chen, S.; Sun, B.; Hong, W.; Aziz, H.; Meng, Y.; Li, Y. Influence of Side Chain Length and Bifurcation Point on the Crystalline Structure and Charge Transport of Diketopyrrolopyrrole-quaterthiophene Copolymers (PDQTs). *J. Mater. Chem. C* **2014**, *2*, 2183−2190.
(27) Chang, J.-F.; Sun, B.; Breiby, D. W.; Nielsen, M. M.; Sölling, T. I.; Giles, M.; McCulloch, I.; Sirringhaus, H. Enhanced Mobility of Poly(3-hexylthiophene) Transistors by Spin-Coating from High-Boiling-Point Solvents. *Chem. Mater.* **2004**, *16*, 4772−4776.
(28) Lee, H. S.; Kim, D. H.; Cho, J. H.; Park, Y. D.; Kim, J. S.; Cho, K. Enhancement of Interconnectivity in the Channels of Pentacene Thin-Film Transistors and Its Effect on Field-Effect Mobility. *Adv. Funct. Mater.* **2006**, *16*, 1859−1864.
(29) Crossland, E. J. W.; Tremel, K.; Fischer, F.; Rahimi, K.; Reiter, G.; Steiner, U.; Ludwigs, S. Anisotropic Charge Transport in Spherulitic Poly(3-hexylthiophene) Films. *Adv. Mater.* **2012**, *24*, 839−844.
(30) Kline, R. J.; McGehee, M. D. Morphology and Charge Transport in Conjugated Polymers. *Polym. Rev.* **2006**, *46*, 27−45.
(31) McCulloch, I.; Heeney, M.; Bailey, C.; Genevicius, K.; Macdonald, I.; Shkunov, M.; Sparrowe, D.; Tierney, S.; Wagner, R.; Zhang, W.; Chabinyc, M. L.; Kline, R. J.; Mcgehee, M. D.; Toney, M. F. Liquid-crystalline Semiconducting Polymers with High Charge-carrier Mobility. *Nat. Mater.* **2006**, *5*, 328−333.
(32) Kim, J.; Baeg, K.-J.; Khim, D.; James, D. T.; Kim, J.-S.; Lim, B.; Yun, J.-M.; Jeong, H.-G.; Amegadze, P. S. K.; Noh, Y.-Y.; Kim, D.-Y. Optimal Ambipolar Charge Transport of Thienylenevinylene-Based Polymer Semiconductors by Changes in Conformation for High-Performance Organic Thin Film Transistors and Inverters. *Chem. Mater.* **2013**, *25*, 1572−1583.

DOI: 10.1021/acsami.5b02265
ACS Appl. Mater. Interfaces 2015, 7, 13431−13439